Heliyon 10 (2024) e25269

Contents lists available at ScienceDirect

Heliyon

journal homepage: www.cell.com/heliyon

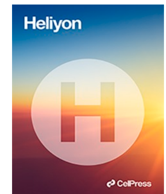

Research article

Effect of multiple quantum well periods on structural properties and performance of extended short-wavelength infrared LEDs

Phuc Dinh Nguyen [a,b,e,1], Minkyeong Kim [a,d,1], Yeongho Kim [c,1], Jiyeon Jeon [a], Suho Park [a,b], Chang Soo Kim [a], Quang Liem Nguyen [e], Byong Sun Chun [a,*], Sang Jun Lee [a,b,**]

[a] *Division of Interdisciplinary Materials Measurement Institute, Korea Research Institute of Standards and Science, Daejeon 34113, Republic of Korea*
[b] *Department of Nano Science, University of Science & Technology, Daejeon 34113, Republic of Korea*
[c] *School of Materials Science & Engineering, Chonnam National University, Gwangju 61186, Republic of Korea*
[d] *Korea Spectral Products, Seoul 08381, Republic of Korea*
[e] *Institute of Materials Science, Vietnam Academy of Science and Technology, Hanoi 10000, Viet Nam*

ARTICLE INFO

Keywords:
Light-emitting diode
Multiple quantum wells
Metamorphic buffer
Extended short wavelength infrared

ABSTRACT

We present research on the role of multiple quantum well periods in extended short-wavelength infrared InGaAs/InAsPSb type-I LEDs. The fabricated LEDs consisted of 6, 15, and 30 quantum well periods, and we evaluated the structural properties and device performance through a combination of theoretical simulations and experimental characterization. The strain and energy band offset was precisely controlled by carefully adjusting the composition of the InAsPSb quaternary material, achieving high valence and conduction band offsets of 350 meV and 94 meV, respectively. Our LEDs demonstrated a high degree of relaxation of 94–96 %. Additionally, we discovered that the temperature-dependent dark current characterization attributed to generation-recombination and trap-assign tunneling, with trap-assign tunneling being more dominant at lower current injections. Electroluminescence analysis revealed that the predominant emission mechanism of the LEDs originated from localized exciton and free exciton radiative recombination, which the 30 quantum wells LED exhibited the highest contribution of the localized exciton/free exciton radiative recombination. We observed that increasing the quantum well periods from 6 to 15 led to an increase in the 300 K electroluminescence intensity of the LED. However, extending the quantum well period to 30 resulted in a decline in emission intensity due to the degradation of the epitaxial film quality.

1. Introduction

Optical sensors are comprised of a photodetector coupled with a light-emitting diode (LED) and can detect and measure gas concentrations based on the absorption signal. Compared to traditional solid-state and chemical sensing technologies, optical sensing

* Corresponding author.
** Corresponding author. Division of Interdisciplinary Materials Measurement Institute, Korea Research Institute of Standards and Science, Daejeon 34113, Republic of Korea.
E-mail addresses: mainue@kriss.re.kr (B.S. Chun), sjlee@kriss.re.kr (S.J. Lee).
[1] These authors contributed equally to this work.

https://doi.org/10.1016/j.heliyon.2024.e25269
Received 11 July 2023; Received in revised form 2 January 2024; Accepted 23 January 2024
Available online 26 January 2024
2405-8440/© 2024 The Authors. Published by Elsevier Ltd. This is an open access article under the CC BY-NC-ND license (http://creativecommons.org/licenses/by-nc-nd/4.0/).

offers the advantages of miniaturization, fast response time, and real-time monitoring. The need for high-quality LEDs operating in the extended short wavelength infrared (e-SWIR, 2–3 μm) region has recently received significant attention due to the absorption lines of many biogases, such as CO_2 and CH_4, falling within this range [1].

GaSb has traditionally been selected as a substrate due to its low lattice mismatch with small bandgap emitters such as InGaAsSb or InAs. In recent years, the adoption of InGaAsSb/AlGaAsSb type-I quantum well (QW) structures have facilitated the emission of wavelengths ranging from 1.5 μm to 3.5 μm [2]. In comparison to GaSb-based devices, InP-based devices have the advantages of low cost, advanced processing technology, and good thermal conductivity. However, lattice-matched LED growth on InP substrates has the drawback of only producing emission wavelengths up to 1.7 μm [3]. To overcome these challenges, extensive research has been

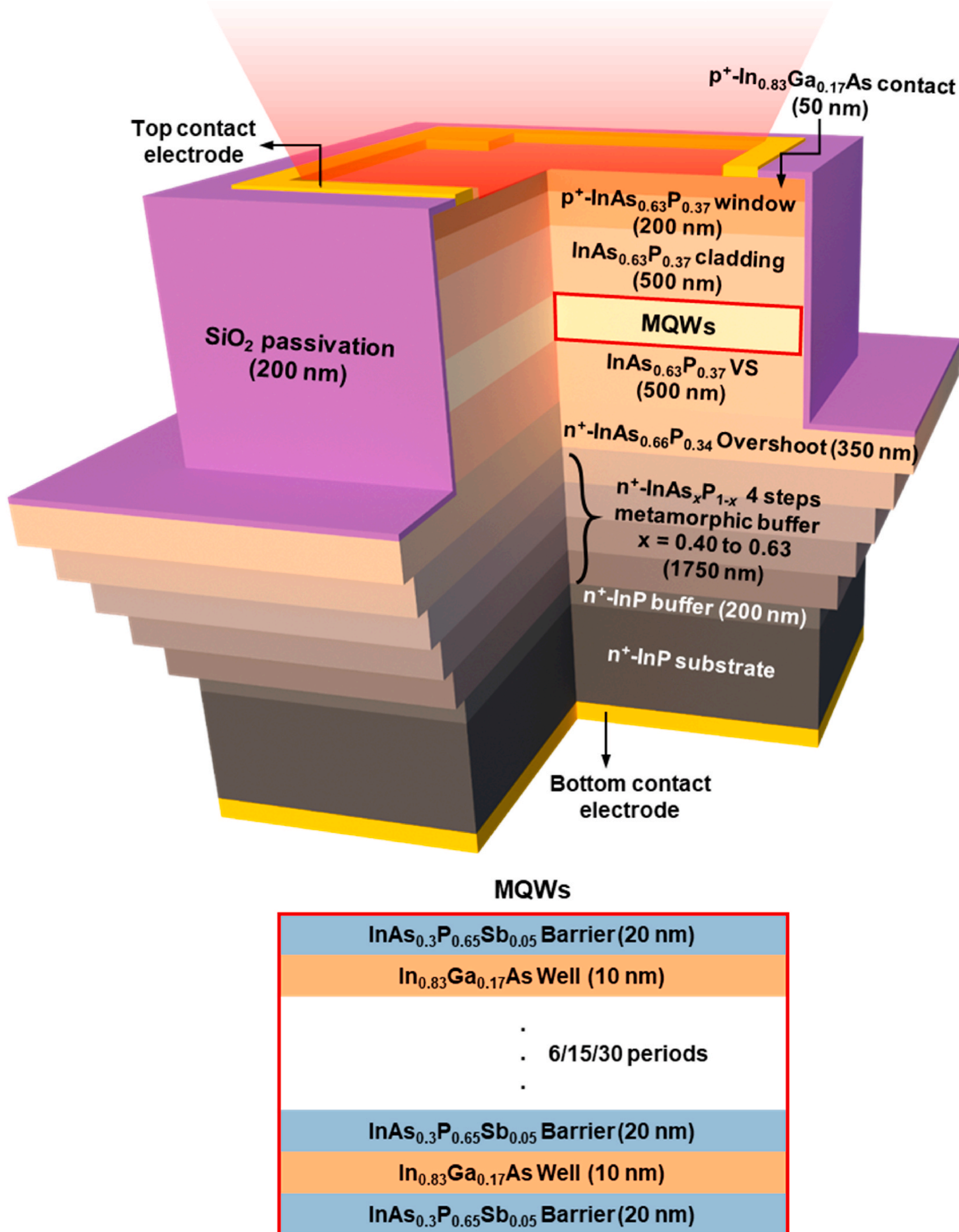

Fig. 1. Schematic structure represents our metamorphic growth e-InGaAs/InAsPSb light emitting diodes grown on InP substrate.

conducted to extend the emission wavelength of InP-based devices. This research has included the use of high-strain InGaSb/InGaAs type-II QWs [4,5] and complex quantum cascade structures [6,7]. However, growing these structures via metal-organic chemical vapor deposition (MOCVD) presents significant challenges.

An alternative method for extending the emission wavelength include using compositionally graded metamorphic buffers to improve the matching to the lattice constant of the InP substrate [8–11]. For example, modified InAs type-I QWs grown on cationic mixed InAlAs metamorphic buffers using molecular beam epitaxy (MBE) have reported emission wavelengths up to 2.9 μm [10,11]. The utilization of MBE for growing strained InAs type-I QWs on a cationic mixed InAlAs metamorphic buffer has demonstrated the ability to extend the emission wavelength up to 2.9 μm. However, a drawback of this structure is that the emission of continuous waves is achieved only up to temperatures of 180 K [10]. $InAs_xP_{1-x}$ anionic mixed metamorphic buffers with lattice matching to InGaAs are considered potential e-SWIR emitters due to their ability to tune the bandgap within the desired wavelength range. These materials have been extensively utilized as photodetectors, demonstrating cutoff wavelengths up to 3.0 μm [12]. However, the realization of InGaAs type-I emitters has been challenging due to the absence of high-quality lattice-matching barriers.

On the other hand, to maximize the external photon emission yield, it is commonly used to increase the period number of the QW to expand the emission cross-section area. Previous studies have shown that increasing the QW period number can hinder the carrier overflow and auger processes and consequently maximize the photon emission yield [13,14]. However, including more layers may also introduce more Shockley-Read-Hall (SHR) centers, which can decrease the rate of radiative recombination [15]. Therefore, the ideal periods of QW for this structure are still uncertain.

In this study, InGaAs/InAsPSb type-I multiple QW (MQW) LEDs were grown utilizing an InAsP anionic mixed metamorphic buffer. In particular, the composition of the InAsPSb quaternary material was carefully controlled to precisely adjust the strain and energy band offset. Both theoretical simulations and experimental characterization were used to investigate the structural properties and device performance as a function of QW periods. Our results indicate that although increasing the QW periods can enhance emission intensity for InGaAs/InAsPSb type-I QWs LED, device performance deteriorates when the QW periods exceed 15 due to degradation in the epitaxial film quality.

2. Experimental procedure

A schematic representing the device structure is shown in Fig. 1. Our LEDs were monolithically grown within a low-pressure MOCVD system on an n^+-InP substrate. Trimethylgallium (TMGa), trimethylindium (TMIn), ashine (AsH_3), and phosphine (PH_3) were employed as sources. Disilane (Si_2H_6) and diethylzinc (DEZn) were used as n-type and p-type dopants, respectively. First, 4 steps n^+-$InAs_xP_{1-x}$ metamorphic buffer with As compositions increase from $x = 0.40$ to 0.63 was grown with a step of $x = 0.058$. The thickness of each step was designed to be 350 nm to ensure crystal relaxation. The composition was tuned by varying the AsH_3 flow

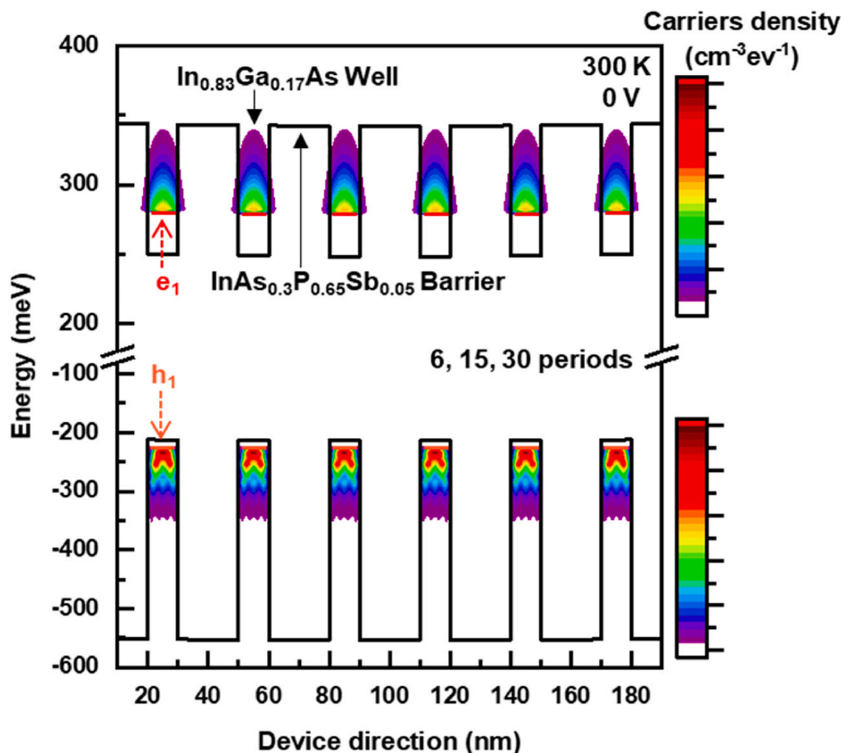

Fig. 2. Simulated band structure and carrier density of the MQW at 300 K and 0 V bias.

rate while keeping PH_3 flow rate constant. To further reduce residual strain and smooth the surface, 350 nm of overshoot n^+-$InAs_{65}P_{35}$ was grown [16]. Then, 500 nm $InAs_{0.63}P_{0.37}$ was grown as a virtual substrate. A series of 3 LEDs were sequentially grown with the active layer consisting of 6, 15, and 30 periods of 10 nm-$In_{0.83}Ga_{0.17}As$/20 nm-$InAs_{0.3}P_{0.65}Sb_{0.05}$ MQWs. The composition and thickness of each layer were carefully designed to minimize the strain with respect to the virtual substrate [17]. After a 500 nm top cladding layer of $InAs_{0.63}P_{0.35}$, we grew 200 nm of p^+-$In_{0.63}P_{0.35}$ to prevent electron overflow. Finally, 50 nm of p^+-$In_{0.83}Ga_{0.17}As$ was grown on top for Ohmic contact.

Devices were fabricated into 300 × 300 μm^2 square mesas using photolithography and dry etching technique. Further H_3PO_4/H_2O_2/H_2O and H_3PO_4/HCl wet etching was performed to eliminate mesa damage from dry etching. The mesa side walls were passivated by 200 nm of SiO_2 using plasma-enhanced chemical vapor deposition and dry etching technique. Pd/Ti/Cr/Au was deposited for top metallization and Pd/Ge/Au was deposited on the back side for bottom metallization using an e-beam evaporation system. After that, fabricated LEDs were packaged into a copper housing, ready for further analysis.

Surface morphology was measured using a Nomarski differential interference contrast microscope system (Leica DM4 M). The crystallographic characterization was performed using a high-resolution X-ray diffraction (X'Pert MRD) system using CuKα1 radiation. The measured spectra were analyzed using X'Pert Epitaxy software to investigate the strain and composition of the LEDs.

Dark current density-voltage characteristic was performed using a source measurement unit (Keithley 236) inside a temperature-controlled liquid N_2-cooled cryostat. For electroluminescence (EL) characteristics, samples were mounted inside a temperature-controlled He_2-cooled cryostat and excited by a current source unit (Keysight B2910BL). Emission photons were collected and analyzed by a Fourier transform infrared spectrometer (Nicolet 6700). For evaluating the dependence of emission intensity on injecting current, emission signals were collected and analyzed by a spectrometer (Horiba iHR-350) equipped with an InGaAs detector and lock-in amplifier.

3. Results and discussion

We first analyzed the electronic structure of the LED's QWs by conducting Nextnano quantum simulations using parameters obtained from the literature [18,19]. The resulting band structure and carrier density at 300 K is shown in Fig. 2.

The simulated valence band and conduction band offsets between the $In_{0.83}Ga_{0.17}As$ well layer and the $InAs_{0.3}P_{0.65}Sb_{0.05}$ barrier layer are 350 meV and 94 meV, respectively. In a type-I QWs structure, a higher band offset is desired in order to efficiently confine the carriers within the low bandgap layer. The thermal energy, calculated using the equation $E(T) = K_BT$, where K_B is Boltzmann constant and T is temperature, is equal to 25 meV at room temperature. The calculated band offset values for the well/barrier structures and compositions we introduced are much higher than the thermal energy, suggesting that our LEDs can operate at room temperature.

We investigated the morphological quality of our LEDs using the Nomarski interference contrast microscope, enhancing the contrast though the differential phase of transmitted light. The results are shown in Fig. 3. The 6 QWs LED and 15 QWs LED exhibited relatively smooth surfaces, whereas oval-shaped defects (~10 μm in size) were observed on the surface of the 30 QWs LED, indicating a degradation in epitaxial film quality.

The reciprocal space map (RSM) of our LEDs measured in the vicinity of the asymmetric reflection (115) shown in Fig. 4. Full relaxation lines presented as dotted lines. The reciprocal lattice unit (r. l. u.) were calculated using equations (1) and (2):

$$Q_x = (2\pi / \lambda_{Xray})[cos(2\theta - \omega) - cos(\omega)] \quad (1)$$

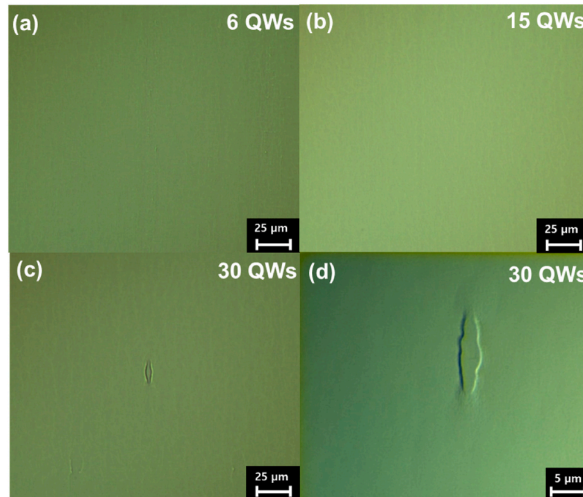

Fig. 3. Nomarski microscopy images of LED with (a) 6 QWs, (b) 15 QWs, and (c) 30 QWs at 20x magnification. (d) Nomarski microscopy image of QWs with 30 QWs at 150x magnification.

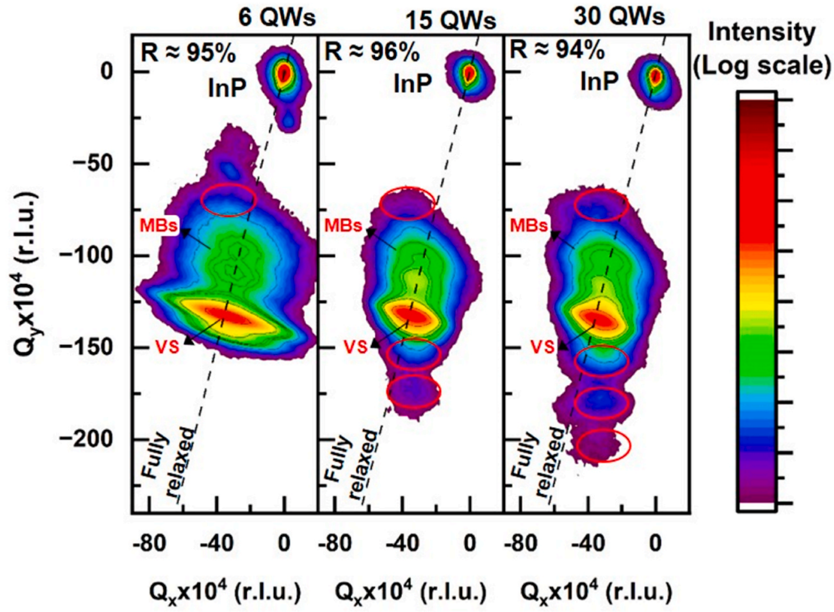

Fig. 4. Reciprocal space maps at the vicinity of the (115) asymmetric reflection of LED with 6 QWs (left), 15 QWs (middle) and 30 QWs (right), respectively. Fully relaxed line is shown.

$$Q_y = (2\pi / \lambda_{Xray})[cos(2\theta - \omega) + sin(\omega)] \tag{2}$$

The reciprocal lattice point (RLP) of the InP substrate defined as the reference ($Q_x = Q_y = 0$). Several RLPs were observed in the RSMs, corresponding to the $InAs_xP_{1-x}$ metamorphic buffers along with $InAs_{0.63}P_{0.37}$ virtual substrates, respectively (indicated as MBs and VS). The out-of-plane and in-plane lattice constants for the $InAs_{0.63}P_{0.37}$ virtual substrates calculated as follows: a (⊥) ≈ 5. 9903 Å/ a (||) ≈ 5.9791 Å, a (⊥) ≈ 5.9897 Å/a (||) ≈ 5.9808 Å, and a (⊥) ≈ 5.9920 Å/a (||) ≈ 5.9782 Å for 6, 15, and 30 QWs LEDs, respectively.

The degree of strain relaxation (*R*) is evaluated using equation (3):

$$R = \frac{(a_{\|} - a_s)}{(a_r - a_s)} \tag{3}$$

Where $a_{\|}$ is the in-plane lattice constant, a_s is InP substrate lattice constant, a_r is the fully relaxed lattice constant. *R* is calculated to be 95, 96, and 94 % for 6, 15, and 30 QWs LED, respectively.

Interestingly, RLPs for $In_{0.83}Ga_{0.17}As/InAs_{0.3}P_{0.65}Sb_{0.05}$ MQWs pendellosung fringes were observed (shown as red ellipses). These RLPs have the same Q_x coordinates as the $InAs_{0.63}P_{0.37}$ virtual substrates, indicating the MQW is strained equally, i.e., has the same in-

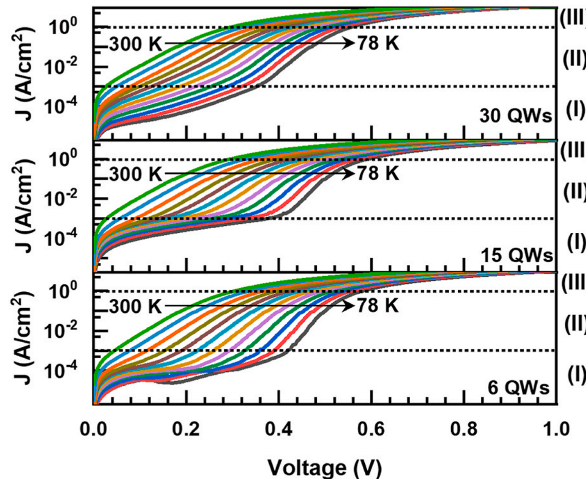

Fig. 5. Forward dark J-V characteristic of LED with 6 QWs (bottom), 15 QWs (middle) and 30 QWs (top), respectively.

plane lattice constant as the virtual substrates. By performing an analysis of the vertical cross-section around the virtual substrates RLPs, the fringes period was estimated to be $\Delta Q_y \approx 0.0024$ r. l.u, corresponding to a period thickness of $\Delta t \approx 31.5$ nm, which is consistent with our growth target QW thickness (as shown in Figs. 1 and 10 nm-$In_{0.83}Ga_{0.17}As$/20 nm-$InAs_{0.3}P_{0.65}Sb_{0.05}$). For 30 QWs LED, these pendellosung fringes are diffused along the in-plane direction (Q_x), evidence of the degradation of the QWs' quality. When the thickness of the QWs stack increases above the critical thickness [17], the accumulated strain is released through the strain relaxation process, resulting in the formation of threading dislocations [20]. These dislocations can disrupt adatom diffusion during growth, generating oval-shaped surface defects, as observed in the 30 QWs LED (Fig. 3(c) and (d)).

Fig. 5 illustrates forward dark J-V characteristics of our LEDs with different QW periods at varying temperatures, plotted on a semi-logarithmic scale. As observed in the figure, there are three distinct regions with different slopes, indicating a bias-dependent dark current mechanism (designated as I: $J < 10^{-4}$ A/cm^2; II: 10^{-4} A/cm$^2 < J < 1$ A/cm^2; III: $J > 1$ A/cm^2).

The dark J-V curve was simulated using equation (4) (Shockley relation):

$$J = J_0 \, exp(qV / E_T) \tag{4}$$

Where J_0 is the pre-exponential factor, q is the fundamental electron charge, and E_T is the characteristic energy associated with the potential barrier for the carrier transition. E_T can also be expressed as $E_T = nk_BT$, where n is the diode ideality factor, T is the temperature, and k_B is the Boltzmann constant. In the well-known Sah-Noyce-Shockley model, the ideality factors 1 and 2 are attributed to the drift-diffusion and generation-recombination (GR) mechanisms, respectively. The diode ideality factor and E_T obtained from each region are presented in Fig. 6(a)-(c).

Across all our LEDs with varying QW periods, a region I is characterized by a high ideality factor, with a value of n ≈ 7 at 78 K. As the temperature increases gradually, n decreases to n ≈ 3 at 300 K. The unrealistically high ideality factor in LEDs is associated with trap-assisted tunneling (TAT) current [21]. The potential barriers for these tunneling events inferred from the E_T. Interestingly, the extracted E_T for all LEDs exhibits a temperature-insensitive value of ≈40 meV. This value is close to the calculated conduction band offset (92 meV) of the QWs, suggesting that the primary tunneling entity may be the escape of electrons through the conduction band barrier assigned by interface localization traps. In region II, the ideality factor is significantly smaller compared to the region I. E_T also exhibited a lower value of 15–30 meV. In this region, the TAT current is suppressed by the GR current. In region III, the series resistance is dominant, as evidenced by the linear J-V relationship (shown in Fig. 5).

Fig. 7(a) shows the electroluminescence (EL) spectra of the LEDs measured at 15 K with an excitation current density of 1 A/cm^2. Two emission bands were observed with Gaussian decay positions at 541 meV/594 meV, 548 meV/590 meV, and 537 meV/593 meV for the 6, 15, and 30 QWs LED, respectively.

To understand the radiative recombination mechanism, we conducted quantum simulations using Nextnano to calculate the optical transition energy. Our results revealed only one electron-confined state (e_1), with an optical transition energy to the first hole-confined state (h_1) of $\Delta E_{e1\text{-}h1} = 595$ meV at 15 K. Therefore, due to the similarity in energy, we assigned the higher energy peak to a free exciton (FE) transition.

In previous studies, multi-band emission behavior at low temperatures has been observed in III-V MQW systems [22–24]. Narukama et al. and Poças et al. suggested that composition inhomogeneities and/or interfacial roughness cause potential fluctuations in the well, creating localization traps near the excitonic density of states' band tails [22,23]. Excited carriers can relax into these localization traps via phonon emission and recombine radiatively to produce lower energy emission bands adjacent to the main emission band. Therefore, the lower energy peak is attributed to the localized exciton (LE) transitions. The LE/FE ratio was calculated to be 0.96 and 0.97 for the 6 and 15 QWs LED, indicating a similar density of potential localizations. Interestingly, the LE/FE ratio for the 30 QWs LED was calculated to be higher at 1.49. This increase is expected because our structural analysis (Figs. 3 and 4) showed that the 30 QWs LED degraded the epitaxial film quality, resulting in a higher density of localization traps.

The EL spectra of the LEDs at 300 K are presented in Fig. 7(b). At this temperature, the LE and FE bands merge, resulting in a broad asymmetric peak. The Gaussian decomposed LE/FE peak positions are 510 meV/537 meV, 515 meV/542 meV, and 511 meV/538 meV for the 6, 15, and 30 QWs LED, respectively. The simulated value of $\Delta E_{e1\text{-}h1}$ is 526 meV at 300 K, agree well to the decomposed FE band

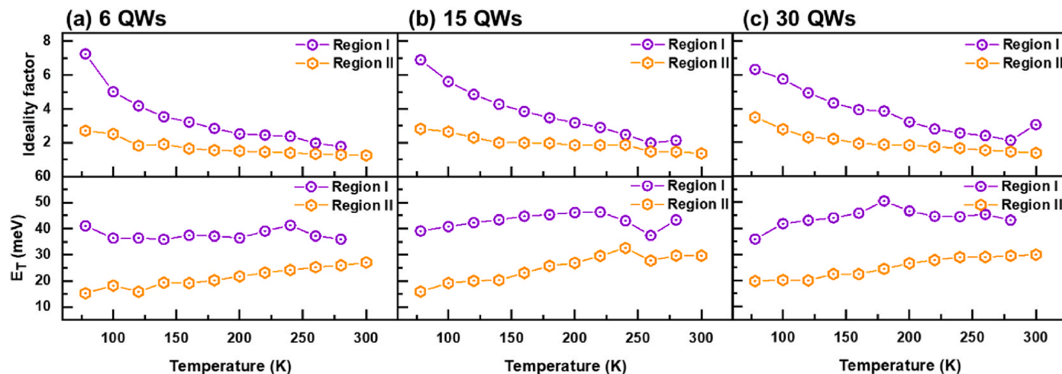

Fig. 6. Extracted ideality factor and their corresponding characteristic energy of LED with: (a) 6 QWs, (b) 15 QWs and (c) 30 QWs, respectively.

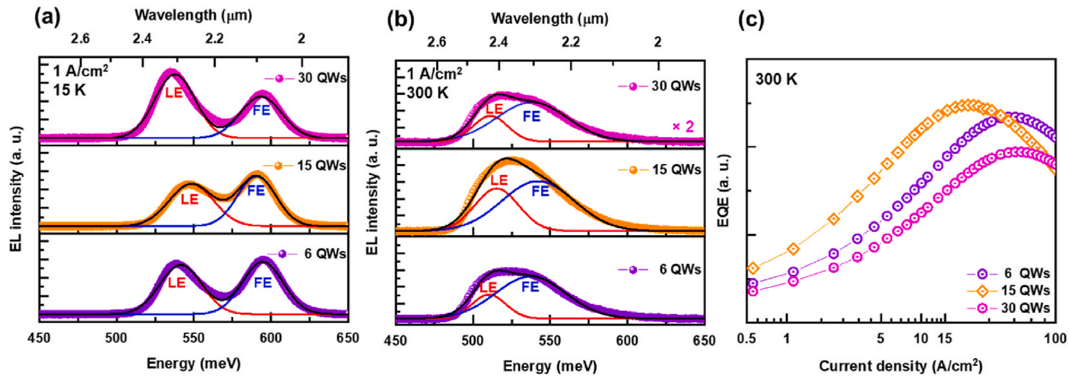

Fig. 7. Electroluminescence spectra, recorded at (a) 15 K and (b) 300 K. (c) relative EQE versus current density.

energy value. As the temperature increases, the localized carriers become thermally excited and move to higher energy states, leading to a band-filling blue shift. This effect competes with the bandgap shrinkage red-shift in the emission energy [23,24]. Since the localization potential confinement is smaller than the well/barrier confinement, the LE band exhibits a more band-filling blue shift compared to the FE band. Consequently, from 15 K to 300 K, the LE band exhibits a smaller net red shift (26–31 meV) compared to the FE band (48–55 meV).

Looking closely at Fig. 7(b), it is evident that the EL intensity does not increase proportionally with QW periods. The 15 QWs LED shows a 1.38-fold increase in integrated EL intensity at 300 K compared to the 6 QWs LED, while the 30 QWs LED exhibits a 0.57-fold decrease in integrated EL intensity.

For further investigation, we investigated relative external quantum efficiency (EQE, Fig. 7(c)) characteristics of our LEDs at 300 K. The relative EQE was calculated using equation (5):

$$EQE \sim L/J \tag{5}$$

Where L is the EL photon output and J is the injection current density [25]. The L-J relation was modeled using equation (6):

$$L = \alpha J^{\beta} \tag{6}$$

Where L is the light output, α is the pre-exponential factor, J is the injection current density, and β is the exponential factor associated with the recombination process [21,26].

The extracted β values in the low current density region are 1.44, 1.29, and 1.49 for 6, 15, and 30 QWs LED, respectively. These values are higher than 1, suggesting a dominance of non-radiative processes [21]. Based on our previous analysis of the forward dark

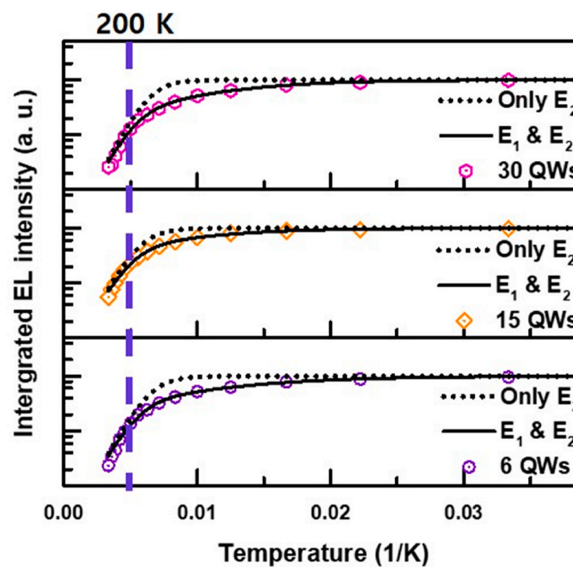

Fig. 8. Arrhenius plot of integrated EL intensity versus inverted temperature of LED with 6 QWs (bottom), 15 QWs (middle) and 30 QWs (top), respectively.

J-V characteristics, it is most likely that TAT is responsible for the behavior observed in the low current density region (as shown in Fig. 6). As the injection current increases, localized trap states become occupied, leading to a super-linear L-J dependence. Consequently, the relative EQE also improves with increasing injection current. However, at high current densities, when the non-radiative trap states become saturated, the extracted β values decrease to 0.83, 0.50, and 0.76 for 6, 15, and 30 QWs LED, respectively. As a result, the EQE will eventually reach a maximum value and then start to decrease. Interestingly, the 15 QWs LED achieves EQE saturation at $J \approx 22$ A/cm^2, whereas the 6 QWs LED reaches EQE saturation at $J \approx 30$ A/cm^2. This suggests that carrier leakage is better suppressed in the 15 QWs LED, likely due to the longer QWs duration. However, in the case of 30 QWs LED, a higher density of local traps, along with a degradation in crystal quality, can lead to an increase in non-radiative centers. As a consequence, both the light intensity and the saturation value of EQE decrease compared to the values observed for the 6 QWs and 15 QWs LEDs.

To examine the thermal quenching mechanism of our LEDs, we plotted the integrated EL intensity against inverse temperature, as shown in Fig. 8. For this analysis, we employed the Arrhenius model, which follows equation (7):

$$I(T) = \frac{I_0}{1 + A\,exp\left(-\frac{E_1}{k_B T}\right) + B\,exp\left(-\frac{E_2}{k_B T}\right)} \tag{7}$$

Here *I(T)* represents the integrated EL at temperature T, while I_0 is the integrated EL at cryogenic temperature, A and B are rate constants, and E_1 and E_2 are the potential barriers for the corresponding thermal quenching process, assuming the presence of two non-radiative channels. The solid lines in the graph provided the best fit results, with $E_1 = 14.05 \pm 0.82$ meV/$E_2 = 85.30 \pm 7.43$ meV for the 6 QWs LED, $E_1 = 16.61 \pm 1.49$ meV/$E_2 = 83.82 \pm 7.57$ meV for the 15 QWs LED, and $E_1 = 16.98 \pm 0.90$ meV/$E_2 = 88.63 \pm 7.57$ meV for the 30 QWs LED. For comparison, the dashed line represents the fit line obtained when considering only E_2.

The results indicate that non-radiative channel E_1 dominates at temperatures below 200 K, while channel E_2 dominates above 200 K. Channel E_1 arises from the thermionic emission of carriers from the localization trap [23,24]. When carriers possess adequate thermal energy, they can escape from the localization trap, rise to a higher energy state, and undergo non-radiative recombination. On the other hand, the value of E_2 is close to the calculated conduction band offset (94 meV), suggesting that the mechanism for this channel is likely the escape of electrons into the energy continuum band associated with interface localization.

4. Conclusions

In this study, InGaAs/InAsPSb type-I MQW LEDs with 6, 15, and 30 QW periods were grown on an InAsP anionic mixed metamorphic buffer. Using an $InAs_{0.3}P_{0.65}Sb_{0.05}$ quaternary barrier, the $In_{0.83}Ga_{0.17}As/InAs_{0.3}P_{0.65}Sb_{0.05}$ MQWs exhibit high valence and conduction band offsets of 350 meV and 94 meV, respectively, enabling effective confinement of carriers within the wells. RSM structure characterization revealed that our LEDs exhibit a high degree of relaxation of 94–96 %. Temperature-dependent dark J-V characterization indicates the dark current mechanism attributed to GR and TAT, with TAT being more dominant at lower current injections. Furthermore, temperature-dependent EL analysis indicates that the main emission mechanism of the LED arises from localized exciton and free exciton recombination, with the LE/FE contribution being the highest in the 30 QWs LED due to the higher localization density. Therefore, increasing the QW periods from 6 to 15 enhances the 300 K EL intensity of the LED, but increasing it further to 30 reduces the emission intensity due to epitaxial film quality degradation. Our findings indicate that the optimal QW period for the e-InGaAs/InAsPSb system we have developed is 15. This study can offer valuable insights for future research and development of e-SWIR MQWs LED.

Data availability

Data will be made available on request.

Additional information

No additional information is available for this paper.

CRediT authorship contribution statement

Phuc Dinh Nguyen: Conceptualization, Data curation, Methodology, Writing – original draft, Writing – review & editing. **Minkyeong Kim:** Conceptualization, Data curation, Methodology, Writing – original draft, Writing – review & editing. **Yeongho Kim:** Conceptualization, Data curation, Methodology, Writing – original draft, Writing – review & editing. **Jiyeon Jeon:** Conceptualization, Data curation, Methodology, Writing – original draft, Writing – review & editing. **Suho Park:** Conceptualization, Data curation, Methodology, Writing – original draft, Writing – review & editing. **Chang Soo Kim:** Conceptualization, Data curation, Methodology, Writing – original draft, Writing – review & editing. **Quang Liem Nguyen:** Conceptualization, Data curation, Methodology, Writing – original draft, Writing – review & editing. **Byong Sun Chun:** Conceptualization, Data curation, Methodology, Writing – original draft, Writing – review & editing. **Sang Jun Lee:** Conceptualization, Data curation, Funding acquisition, Methodology, Writing – original draft, Writing – review & editing.

Declaration of competing interest

The authors declare the following financial interests/personal relationships which may be considered as potential competing interests:Sang Jun Lee reports financial support was provided by Korea Ministry of Trade Industry and Energy. Sang Jun Lee reports financial support was provided by National Research Foundation of Korea.

Acknowledgments

This research was supported by Nano·Material Technology Development Program through the National Research Foundation of Korea (NRF) funded by Ministry of Science and ICT (NRF-2018M3A7B4069994). This research was supported by National R&D Program through the National Research Foundation of Korea (NRF) grant funded by the Korea government(MSIT) (2022M3I8A2079227, NRF-2022M3H4A1A02076394, and RS-2023-00234859). This work was supported by the Technology Innovation Program (10052824, Development of the Sb based semiconductor epitaxy for mid-infrared light emitting diode) funded by the Ministry of Trade, Industry & Energy (MOTIE, Korea).

References

[1] S. Stephan, D. Frederic, A. Markus-Christian, Novel InP- and GaSb-based light sources for the near to far infrared, Semicond. Sci. Technol. 31 (2016), https://doi.org/10.1088/0268-1242/31/11/113005.
[2] S. Suchalkin, S. Jung, G. Kipshidze, L. Shterengas, T. Hosoda, D. Westerfeld, D. Snyder, G. Belenky, GaSb based light emitting diodes with strained InGaAsSb type I quantum well active regions, Appl. Phys. Lett. 93 (2008) 81107, https://doi.org/10.1063/1.2974795.
[3] E.H. Li, Material parameters of InGaAsP and InAlGaAs systems for use in quantum well structures at low and room temperatures, Phys. E Low-Dimensional Syst. Nanostructures. 5 (2000) 215–273, https://doi.org/10.1016/S1386-9477(99)00262-3.
[4] S. Sprengel, C. Grasse, K. Vizbaras, T. Gruendl, M.-C. Amann, Up to 3 μm light emission on InP substrate using GaInAs/GaAsSb type-II quantum wells, Appl. Phys. Lett. 99 (2011) 221109, https://doi.org/10.1063/1.3665256.
[5] S. Sprengel, A. Andrejew, K. Vizbaras, T. Gruendl, K. Geiger, G. Boehm, C. Grasse, M.-C. Amann, Type-II InP-based lasers emitting at 2.55 μm, Appl. Phys. Lett. 100 (2012) 41109, https://doi.org/10.1063/1.3679378.
[6] N. Bandyopadhyay, Y. Bai, S. Tsao, S. Nida, S. Slivken, M. Razeghi, Room temperature continuous wave operation of λ ~ 3–3.2 μm quantum cascade lasers, Appl. Phys. Lett. 101 (2012) 241110, https://doi.org/10.1063/1.4769038.
[7] D.G. Revin, J.W. Cockburn, M.J. Steer, R.J. Airey, M. Hopkinson, A.B. Krysa, L.R. Wilson, S. Menzel, InGaAs/AlAsSb/InP quantum cascade lasers operating at wavelengths close to 3μm, Appl. Phys. Lett. 90 (2007) 21108, https://doi.org/10.1063/1.2431035.
[8] D. Jung, Y. Song, L. Yu, D. Wasserman, M. Larry Lee, 2.8 μm emission from type-I quantum wells grown on InAsxP1−x/InP metamorphic graded buffers, Appl. Phys. Lett. 101 (2012) 251107, https://doi.org/10.1063/1.4773024.
[9] D. Jung, L. Yu, S. Dev, D. Wasserman, M.L. Lee, Room-temperature mid-infrared quantum well lasers on multi-functional metamorphic buffers, Appl. Phys. Lett. 109 (2016) 211101, https://doi.org/10.1063/1.4968560.
[10] Y. Gu, Y.G. Zhang, Y.J. Ma, L. Zhou, X.Y. Chen, S.P. Xi, B. Du, InP-based type-I quantum well lasers up to 2.9 μm at 230 K in pulsed mode on a metamorphic buffer, Appl. Phys. Lett. 106 (2015) 121102, https://doi.org/10.1063/1.4916270.
[11] Y.Y. Cao, Y.G. Zhang, Y. Gu, X.Y. Chen, L. Zhou, H. Li, 2.7 μm InAs quantum well lasers on InP-based InAlAs metamorphic buffer layers, Appl. Phys. Lett. 102 (2013) 201111, https://doi.org/10.1063/1.4807671.
[12] S. Park, J. Jeon, V.M. More, R.S. Lee, Y. Seo, M. Kim, P.D. Nguyen, M. Kim, J.S. Kim, Y. Kim, S.J. Lee, Monolithic two-color short-wavelength InGaAs infrared photodetectors using InAsP metamorphic buffers, Appl. Surf. Sci. 581 (2022) 152421, https://doi.org/10.1016/j.apsusc.2022.152421.
[13] Y.P. Zhang, Z.-H. Zhang, W. Liu, S.T. Tan, Z.G. Ju, X.L. Zhang, Y. Ji, L.C. Wang, Z. Kyaw, N. Hasanov, B.B. Zhu, S.P. Lu, X.W. Sun, H.V. Demir, Nonradiative recombination critical in choosing quantum well number for InGaN/GaN light-emitting diodes, Opt Express 23 (2015) A34–A42, https://doi.org/10.1364/OE.23.000A34.
[14] C.S. Xia, Z.M. Simon Li, Z.Q. Li, Y. Sheng, Z.H. Zhang, W. Lu, L.W. Cheng, Optimal number of quantum wells for blue InGaN/GaN light-emitting diodes, Appl. Phys. Lett. 100 (2012) 263504, https://doi.org/10.1063/1.4731625.
[15] N.I. Bochkareva, Y.T. Rebane, Y.G. Shreter, Increase in the Shockley–Read–Hall recombination rate in InGaN/GaN QWs as the main mechanism of the efficiency droop in LEDs at high injection levels, Semiconductors 49 (2015) 1665–1670, https://doi.org/10.1134/S1063782615120040.
[16] J. Tersoff, Dislocations and strain relief in compositionally graded layers, Appl. Phys. Lett. 62 (1993) 693–695, https://doi.org/10.1063/1.108842.
[17] N.J. Ekins-Daukes, K. Kawaguchi, J. Zhang, Strain-balanced criteria for multiple quantum well structures and its signature in X-ray rocking curves, Cryst. Growth Des. 2 (2002) 287–292, https://doi.org/10.1021/cg025502y.
[18] S. Birner, T. Zibold, T. Andlauer, T. Kubis, M. Sabathil, A. Trellakis, P. Vogl, Nextnano: general purpose 3-D simulations, IEEE Trans. Electron. Dev. 54 (2007) 2137–2142, https://doi.org/10.1109/TED.2007.902871.
[19] I. Vurgaftman, J.R. Meyer, L.R. Ram-Mohan, Band parameters for III–V compound semiconductors and their alloys, J. Appl. Phys. 89 (2001) 5815–5875, https://doi.org/10.1063/1.1368156.
[20] E.A. Fitzgerald, Dislocations in strained-layer epitaxy: theory, experiment, and applications, Mater. Sci. Rep. 7 (1991) 87–142, https://doi.org/10.1016/0920-2307(91)90006-9.
[21] X.A. Cao, E.B. Stokes, P.M. Sandvik, S.F. LeBoeuf, J. Kretchmer, D. Walker, Diffusion and tunneling currents in GaN/InGaN multiple quantum well light-emitting diodes, IEEE Electron. Device Lett. 23 (2002) 535–537, https://doi.org/10.1109/LED.2002.802601.
[22] Y. Narukawa, Y. Kawakami, S. Fujita, S. Fujita, S. Nakamura, Recombination dynamics of localized excitons in In0.20Ga0.80N-In0.05Ga0.95N multiple quantum wells, Phys. Rev. B 55 (1997) R1938–R1941, https://doi.org/10.1103/PhysRevB.55.R1938.
[23] L.C. Poças, J.L. Duarte, E.M. Lopes, I.F.L. Dias, E. Laureto, D.F. César, J.C. Harmand, The effect of potential fluctuations on the optical properties of InGaAs/InGaAlAs single and coupled double quantum wells, J. Appl. Phys. 100 (2006) 53519, https://doi.org/10.1063/1.2260826.
[24] Y. Wang, X. Sheng, Q. Guo, X. Li, S. Wang, G. Fu, Y.I. Mazur, Y. Maidaniuk, M.E. Ware, G.J. Salamo, B. Liang, D.L. Huffaker, Photoluminescence study of the interface fluctuation effect for InGaAs/InAlAs/InP single quantum well with different thickness, Nanoscale Res. Lett. 12 (2017) 229, https://doi.org/10.1186/s11671-017-1998-8.
[25] M. Shatalov, W. Sun, R. Jain, A. Lunev, X. Hu, A. Dobrinsky, Y. Bilenko, J. Yang, G.A. Garrett, L.E. Rodak, M. Wraback, M. Shur, R. Gaska, High power AlGaN ultraviolet light emitters, Semicond. Sci. Technol. 29 (2014) 84007, https://doi.org/10.1088/0268-1242/29/8/084007.
[26] J.B. Wang, D. Ding, S.R. Johnson, S.Q. Yu, Y.H. Zhang, Determination and improvement of spontaneous emission quantum efficiency in GaAs/AlGaAs heterostructures grown by molecular beam epitaxy, Phys. Status Solidi 244 (2007) 2740–2751, https://doi.org/10.1002/pssb.200675612.